Engineering Structures
Supports open access

9.2
CiteScore

5.5
Impact Factor

Volume 262

1 July 2022

Full text access

Editorial Board

Article 114438

View PDF

Research article ○ Abstract only

Use of rubberized engineered cementitious composite in strengthening flexural concrete beams

Basem H. AbdelAleem, Assem A.A. Hassan

Article 114304

Article preview

Research article ○ Abstract only

Dynamic crushing of uniform and functionally graded origami-inspired cellular structure fabricated by SLM

Qixun Li, Xudong Zhi, Feng Fan

Article 114327

Article preview

Research article ○ Abstract only

Two-Direction Shear-Force sensor (2D-SFS) for measurement of friction force in structural Compression–Shear testing

Cao Yingri, Wang Haishen, Sun Jiangbo, Pan Peng

Article 114284

Article preview

Research article ○ Abstract only

On the use of a Pseudo-spectral method in the Asymptotic Numerical Method for the resolution of the Ginzburg–Landau envelope equation

Mohamed Drissi, Mohamed Mansouri, Said Mesmoudi, Khalid Saadouni
Article 114236

Article preview

Research article ○ Abstract only

Recovery stress effect of crimped NiTi SMA fibers on dynamic direct tensile behavior of mortar with considering fiber volume fraction

Eunsoo Choi, Jongkwon Choi, Junwon Seo
Article 114328

Article preview

Research article ○ Abstract only

Accurate structural displacement monitoring by data fusion of a consumer-grade camera and accelerometers

Tong Wu, Liang Tang, Shuai Shao, Xiangyu Zhang, ... Xiaolei Qi
Article 114303

Article preview

Research article ○ Abstract only

Finite element formulation for distortional lateral buckling of I-beams

Ramin Arizou, Magdi Mohareb
Article 114265

Article preview

Research article ○ Abstract only

Analytical-Based application software for Estimating remaining fatigue life of Non-Cantilevered sign structures

Husam A. Alshareef, Khalid W. Al Shboul, Hayder A. Rasheed, Alaaeldin Abouelleil
Article 114315

Article preview

Research article ○ Abstract only

Experimental calibration of a one degree of freedom biodynamic model to simulate human walking-structure interaction

Michèle Schubert Pfeil, Wendell Diniz Varela, Natasha de Paula Amador da Costa
Article 114330

Article preview

Research article ○ Abstract only

A novel crank inerter with simple realization: Constitutive model, experimental investigation and effectiveness assessment

Li Zhang, Songtao Xue, Ruifu Zhang, Linfei Hao, ... Liyu Xie
Article 114308

Article preview

Research article ○ Abstract only

Coupled hygro-mechanical meso-scale analysis of long-term creep and shrinkage of concrete cylinder

Joško Ožbolt, Serena Gambarelli, Sekandar Zadran
Article 114332

Article preview

Research article ○ Abstract only

Reliability assessment of a continuous bridge beam with exposed reinforcement

M.G. Parmiani, L. Orta
Article 114281

Article preview

Research article ○ Abstract only

Long-term mechanical behaviors of uncracked concrete beams prestressed with external basalt fiber-reinforced polymer tendons

Jianzhe Shi, Xin Wang, Zhishen Wu, Xing Wei, Xiaoguang Ma
Article 114309

Article preview

Research article ○ Abstract only

Fragility analysis of a pipeline under slope failure-induced displacements occurring parallel to its axis

Angelos Tsatsis, Antonios Alvertos, Nikos Gerolymos
Article 114331

Article preview

Research article ○ Abstract only

Bayesian updating for nuclear containment buildings using both mechanical and hydraulic monitoring data

D. Rossat, J. Baroth, M. Briffaut, F. Dufour, ... S. Michel-Ponnelle
Article 114294

Article preview

Research article ○ Abstract only

Effect of partition walls on the seismic response of mass-timber buildings with a post-tensioned rocking wall system

Hamed Hasani, Keri L. Ryan

Article 114316

Article preview

Research article ○ Abstract only

Seismic behavior of damaged RC columns repaired with FRCM composites

Klajdi Toska, Lorenzo Hofer, Flora Faleschini, Mariano Angelo Zanini, Carlo Pellegrino

Article 114339

Article preview

Research article ○ Abstract only

An examination of the size effect in quasi-brittle materials using a bond-based peridynamic model

Mark Hobbs, Tim Dodwell, Gabriel Hattori, John Orr

Article 114207

Article preview

Research article ○ Abstract only

3D interaction diagrams for symmetrically reinforced concrete square sections with various reinforcement ratios

Androniki-Anna Doulgeroglou, Panagiotis Kotronis, Giulio Sciarra, Catherine Bouillon

Article 114272

Article preview

Review article ○ Abstract only

Bending stiffness prediction to mass timber panel-concrete composite floors with notched connections

Lei Zhang, Jianhui Zhou, Sigong Zhang, Ying Hei Chui
Article 114354

Article preview

Research article ○ Abstract only

Axial compression and bond behaviour of recycled aggregate concrete-filled stainless steel tubular stub columns

Lin-Hai Han, Chuan-Yang Xu, Chao Hou
Article 114306

Article preview

Research article ○ Abstract only

Data and evaluation model for the description of the static–dynamic interface between trains and railway bridges

Günther Grunert
Article 114335

Article preview

Research article ○ Abstract only

Maximizing buckling load of elliptical composite cylinders using lamination parameters

Yanan Guo, Gokhan Serhat, Marta Gil Pérez, Jan Knippers
Article 114342

Article preview

Research article ○ Abstract only

Enhancement of punching strength in GFRP reinforced single footings by means of handmade GFRP shear bands

Alireza Doostmohamadi, Mohammad Karamloo, Asghar Vatani Oskouei, Milad Shakiba, Ali Kheyroddin
Article 114349

Article preview

Research article ○ Abstract only

Estimation of bond strength between UHPC and reinforcing bars using machine learning approaches

Zhijie Li, Jianan Qi, Yuqing Hu, Jingquan Wang
Article 114311

Article preview

Research article ○ Abstract only

Lifetime seismic performance assessment on post-tensioned self-centering concrete frames considering long-term prestress loss

Lu-Xi Li, Chao Li, Hong-Nan Li, Hong Hao
Article 114321

Article preview

Research article ○ Abstract only

Fuzzy probabilistic evaluation of soil-structure interaction effects on the soft-first-story structures

Mohammad Seddiq Eskandari Nasab, Jinkoo Kim
Article 114348

Article preview

Research article ○ Abstract only

Thunderstorm wind load evaluation on storm shelters using wind tunnel testing

Tarek Ghazal, Moustafa Aboutabikh, Haitham Aboshosha, Mohamed Abdelwahab
Article 114350

Article preview

Research article ○ Abstract only

Multivariate structural seismic fragility analysis and comparative study based on moment estimation surrogate model and Gaussian copula function

Yexiang Yan, Hongwei Huang, Limin Sun
Article 114324

Article preview

Research article ○ Abstract only

Probabilistic-based nonlinear stability analysis of randomly reinforced microshells under combined axial-lateral load using meshfree strain gradient formulations

Jianguo Zhao, Ju Wang, Saeid Sahmani, Babak Safaei
Article 114344

Article preview

Research article ○ Abstract only

Advances in the application of the Principal Static Wind Loads: A large-span roof case

Giorgio Frontini, Tommaso Argentini, Lorenzo Rosa, Daniele Rocchi
Article 114314

Article preview

Research article ○ Abstract only

An experimental investigation into the shock response of a compact wire rope isolator in its axial direction

D.F. Ledezma-Ramírez, P.E. Tapia-González, M.J. Brennan, P.J. Paupitz Gonçalves
Article 114317

Article preview

Research article ○ Abstract only

Damage evaluation of fixed beams at both ends for bridge health monitoring using a combination of a vibration sensor and a surface acoustic wave device

Shinji Baba, Jun Kondoh
Article 114323

Article preview

Research article ○ Abstract only

Simple rebar anchorage slip macromodel considering corrosion

Ahmad Soraghi, Qindan Huang
Article 114357

Article preview

Research article ○ Abstract only

Flexural behavior of RC beams strengthened with fully or partially prestressed near-surface mounted FRP strips: An experimental investigation

Miao Su, Shuang Gong, Yong Liu, Hui Peng
Article 114345

Article preview

Research article ○ Abstract only

Behaviour of RC beams strengthened in flexure with hybrid CFRP-reinforced UHPC overlays

Majid M.A. Kadhim, Akram Jawdhari, Wissam Nadir, Lee S. Cunningham

Article 114356

Article preview

Research article ○ Abstract only

A novel eddy current damper system for multi-mode high-order vibration control of ultra-long stay cables

Yafei Wang, Zhengqing Chen, Chao Yang, Zhiwen Liu, ... Zhouquan Feng

Article 114319

Article preview

Research article ● *Open access*

Analysing local failure scenarios to assess the robustness of steel truss-type bridges

Giacomo Caredda, M. Cristina Porcu, Manuel Buitrago, Elisa Bertolesi, José M. Adam

Article 114341

View PDF Article preview

Research article ○ Abstract only

Pounding performance between a seismic-isolated long-span girder bridge and its approaches

Wei Guo, Jianzhong Li, Zhongguo Guan, Xu Chen

Article 114397

Article preview

Research article ○ Abstract only

Development of dual-parameter loading protocols for buckling-restrained braced RC frames considering variable axial loads

Jiulin Bai, Huiming Chen, Shuangshuang Jin, Tao You
Article 114388

Article preview

Research article ○ Abstract only

Broadband wave attenuation and topological transport in novel periodic pile barriers

Anchen Ni, Zhifei Shi
Article 114378

Article preview

Research article ○ Abstract only

Dynamic impact of automated truck platooning on highway bridges

Tianyang Ling, Ran Cao, Lu Deng, Wei He, ... Wenjie Zhong
Article 114326

Article preview

Research article ○ Abstract only

Time-dependent strains of prestressed concrete containment vessels: Validation of analytical model by real-world data

Petr Bílý, Adéla Kapicová, Jakub Holan
Article 114403

Article preview

Research article ○ Abstract only

Wind loads prediction using LES: Inflow generation, accuracy and cost assessment for the case of Torre Gioia 22

Jin Xing, Luca Patruno, Chiara Pozzuoli, Gonçalo Pedro, ... Francesco Ubertini
Article 114292

Article preview

Research article ○ Abstract only

A novel tension strap connection for rapid assembly of temporary timber structures

Zhuo-Yang Xin, Kim Baber, Joseph M. Gattas
Article 114320

Article preview

Research article ○ Abstract only

Prediction of buckling capacity of liquid-filled steel conical tanks considering field-measured imperfections

H. Zhang, A.M. El Ansary, W. Zhou
Article 114351

Article preview

Research article ○ Abstract only

Double-resonator based metaconcrete composite slabs and vibration attenuation mechanism

Yang Liu, Dongyu Shi, Huguang He, Sanfeng Liu, Hualin Fan
Article 114392

Article preview

Research article ○ Abstract only

New precast self-centering rocking shear wall with multiple hinged joints: Description and design approach for seismic protection of buildings

Zhipeng Zhai, Wei Guo, Yanhui Liu, Yuhong Ma, Fulin Zhou
Article 114401

Article preview

Research article ○ Abstract only

Measuring support reactions and damage detection in steel beams using distributed strain sensing

Jack GILLHAM, Evan C. BENTZ, Neil A. HOULT
Article 114389

Article preview

Research article ○ Abstract only

Nonlinear truss modeling method for masonry-infilled reinforced concrete frames

Daniel Salinas, Ioannis Koutromanos, Roberto T. Leon
Article 114329

Article preview

Research article ○ Abstract only

A novel enhanced anti-tetra-missing rib auxetic structure with tailorable in-plane mechanical properties

Yilin Zhu, Songhui Jiang, Fucong Lu, Xin Ren
Article 114399

Article preview

Research article ○ Abstract only

Vertical shear capacity of steel-concrete composite deck slabs with steel ribs

Da Xiang, Yuqing Liu, Yichi Shi, Xiaoqing Xu
Article 114396

Article preview

Research article ○ Abstract only

Numerical investigation on the seismic behaviour of GFRP-reinforced concrete rectangular columns

Yasser M. Selmy, Ehab F. El-Salakawy
Article 114355

Article preview

Research article ○ Abstract only

Modelling of in-plane seismic behaviour of one-way steel or timber jack arch floors in existing buildings. Application to the Eixample district of Barcelona

Sara Dimovska, Savvas Saloustros, Luca Pelà, Pere Roca
Article 114343

Article preview

Research article ○ Abstract only

Static bond performance between BFRP bars and concrete with stirrup confinement: A refined modelling

Ping Li, Liu Jin, Renbo Zhang, Xiuli Du
Article 114379

Article preview

Research article ○ Abstract only

Experimental investigation of flexural behaviours of hybrid engineered cementitious composite beams under static and fatigue loading

Shiyao Zhu, Y.X. Zhang, C.K. Lee
Article 114369

Article preview

Research article ○ Abstract only

Influence of ground motion duration on seismic performance of RC frame isolated by high damping rubber bearings

Tao Li, Yijian Yang, Kaoshan Dai, Qingzi Ge, Jianze Wang
Article 114398

Article preview

< Previous vol/issue

Next vol/issue >

ISSN: 0141-0296

ELSEVIER

Engineering Structures 262 (2022) 114329

Contents lists available at ScienceDirect

Engineering Structures

journal homepage: www.elsevier.com/locate/engstruct

Nonlinear truss modeling method for masonry-infilled reinforced concrete frames

Daniel Salinas [a], Ioannis Koutromanos [b,*], Roberto T. Leon [c]

[a] Department of Civil Engineering, Minuto de Dios University, Bogotá 111021, Colombia
[b] Department of Civil and Environmental Engineering, Virginia Polytechnic Institute and State University, 103 Patton Hall, Blacksburg, VA 24061, United States
[c] Department of Civil and Environmental Engineering, Virginia Polytechnic Institute and State University, 102-D Patton Hall, Blacksburg, VA 24061, United States

ARTICLE INFO

Keywords:
Masonry
Infill walls
Non-ductile
Reinforced concrete frames
Truss model
Zero-length macroelement

ABSTRACT

This paper presents a new modeling approach for masonry-infilled, reinforced concrete (RC) frames, based on the nonlinear truss analogy. The unreinforced masonry infill walls are modeled with truss cells containing horizontal, vertical and inclined elements. Zero-length macroelements are also used to account for the localized damage on mortar joints. The frame members are modeled with a recently proposed scheme that can account for inelastic response and can capture the effect of shear damage and failure of RC columns. The modeling approach is validated through analysis of experimentally tested masonry-infilled frames, and its capability in capturing the strength and damage patterns is evaluated. A sensitivity study is also provided, to elucidate the impact of several model parameters on the obtained analytical results.

1. Introduction

Masonry-infilled reinforced concrete frames are a common type of construction in the United States, Eastern Europe, Asia and Latin America. The interaction between the frame and the infill walls typically increases the lateral resistance of the system. This increase of resistance can be beneficial for old construction, which is usually not designed for the level of seismic intensity of modern standards. However, the interaction of the frame with the infill walls may also lead to undesired patterns such as soft-story modes and brittle shear failures in the frame columns. Experimental research (e.g., [36,51,27] has provided valuable data for the performance of infilled RC frames and for the effectiveness of retrofit techniques. However, it is not possible to conduct large-scale tests for a sufficiently wide range of structural configurations and loading scenarios. This means that analytical simulation methods are necessary for the systematic, computational performance assessment of infilled RC frames.

The simplest type of modeling approach for masonry-infilled frames is based on the representation of the infill walls with equivalent struts. This approach, originally proposed by Polyakov [43], has been the focus of a significant amount of work [21,48,31,22,55,20,52,28,7,9] . Klingner and Bertero [22] used strut-based models for infilled frame specimens that were experimentally tested. Al-Chaar [1] conducted nonlinear static analysis with equivalent strut models to investigate the behavior of RC frames with brick infills. He proposed guidelines to determine the expected location of plastic hinges in the frame members, the lengths of the rigid-end zones associated with contact between the frame and infill wall, the effect of openings and partial infills, and the combined effect of in- and out-of-plane loads. Di Trapani et al. [14] proposed a macroelement based on the equivalent strut concept to describe the behavior of infilled frames under combined in-plane and out-of-plane seismic loads. The macroelement consisted of diagonal, vertical and horizontal elements with a fiber section. Hak et al. [18] used equivalent strut models for the prediction of inter-story drifts in infilled frames. Huang et al. [19] used the results of 113 infilled frame experiments in the literature to calibrate a backbone curve for equivalent strut models.

The equivalent strut method provides a simple procedure to account for the effect of masonry infills. Several codes and evaluation guidelines, such as the MSJC code [39] and the ASCE/SEI 41 document [3] include procedures for the analysis and design of infilled frames with equivalent strut models. Given their computational efficiency, such models are well-suited for parametric studies for the seismic performance assessment of infilled frames [10,46,41]. However, an equivalent strut is an over-simplification of the actual behavior of an infill wall and may not properly capture some key aspects of behavior, as explained in Koutromanos and Shing [24]. For instance, a strut model cannot accurately describe column shear failures which may be caused by the frame-to-

* Corresponding author.

https://doi.org/10.1016/j.engstruct.2022.114329
Received 21 August 2021; Received in revised form 16 March 2022; Accepted 24 April 2022
Available online 19 May 2022

infill interaction. An earlier study by Hashemi and Mosalam [20] compared the recorded response of a shake-table specimen which included an unreinforced masonry infill with the corresponding results of a strut-based model. They concluded that improvements were necessary in the specific modeling approach, since it did not give very accurate results for the test that led to significant damage in the infill wall. Stavridis [49] has demonstrated (by means of nonlinear finite element analyses) that the compressive stress field in a masonry infill wall may not be accurately represented by a single diagonal strut and that a strut model ignores the shear transfer between the beam and the infill. Hence, replacing a wall by a diagonal strut will not lead to a realistic representation of the load transfer from the frame to the wall. This has motivated several researchers (e.g., [12,14,15,9]) to pursue multi-strut models to better represent the behavior of infilled frames. While some studies (e.g., [4]) have shown that multiple struts may improve the accuracy of analyses based on the equivalent strut concept, the additional complications introduced by a multi-strut approach may not warrant the development and extensive use of such models.

To address the limitations of the equivalent strut concept, many studies have pursued the analysis of infilled RC frames with refined, nonlinear finite element models [37,2,50,26,45,8]. Such models typically combine continuum, smeared-crack formulations to capture the behavior of the concrete and brick materials, with discrete-cohesive crack elements to account for localized damage along the mortar joints and brick-to-infill interfaces. Special attention is required for capturing the effect of column shear failures, which is usually accomplished through cohesive-crack interface elements. The vast majority of nonlinear finite element analysis efforts have been focused on monotonic loading. Koutromanos et al. [26] have validated the capability of their finite element analysis scheme to capture the in-plane response and damage of infilled frames under cyclic loading. Koutromanos and Shing [25] formulated and validated finite element models for the simulation of infilled frames retrofitted with overlays of composite materials on the infill walls. A similar modeling approach has been used by Redmond et al. [44] for the nonlinear static analysis of infilled RC frames with overlays of mesh-reinforced mortar.

Despite their demonstrated accuracy, refined finite element models are conceptually complicated, because they require the use of special formulations such as discrete-cohesive crack interface elements, and constitutive laws which involve many parameters to be calibrated. Furthermore, finite element analyses are computationally demanding, which means that it may be difficult – if at all possible – to conduct systematic parametric studies of prototype, multi-story structures with finite elements.

Based on the above, there is still a need for an analysis method for infilled RC frames, which will be conceptually simpler and algorithmically more efficient than finite element models, yet more accurate than the somehow crude equivalent-strut models. The present study is aimed to provide such an analysis method, based on the nonlinear truss analogy. A recently proposed truss modeling approach, which is capable of capturing the inelastic response and shear failure of RC components, is used for the frame members. Truss elements are also used to model the brick units of the unreinforced masonry infills. Special, zero-length macroelements are formulated and calibrated to account for localized damage in mortar joints and frame-to-infill interfaces. The number of the model parameters is kept to a minimum, to facilitate calibration with material test data. The capability of the method to capture the response of infilled RC frames, including potential shear failure at the columns, is validated through analyses of experimental tests from the literature.

2. Description of analysis method

The proposed modeling approach constitutes an extension of the method by Moharrami et al. [38] for the analysis of shear-critical RC columns with a rectangular cross-section. This previous method has been shown to be capable of capturing the hysteretic response and damage pattern of columns, including cases involving strength degradation due to shear failures. The method is extended to simulate the behavior of infill walls, by capturing the inelastic response of masonry under compressive stress, and the localized damage along mortar joints and infill-to-frame interfaces. The constitutive models and element formulations described in this section are available in the open-source software *OpenSees* [34], which has been used for the analyses in this paper.

A description of the modeling approach and the process to determine the truss representation of RC members are given in Moharrami et al. [38]. A brief overview is provided here for completeness. The RC components are represented by an assemblage of truss cells, with each cell consisting of two horizontal, two vertical and two diagonal truss elements. Additional horizontal and vertical elements are provided to represent the longitudinal and transverse reinforcement of the various RC components. A summary of the process to establish the planar truss representation of an RC column with a cross-sectional depth h and an out-of-plane sectional thickness t is presented in Fig. 1. As shown in the specific figure, the sectional width, b_d, of the inclined truss elements is determined from the dimensions of the truss cell and the value of the inclination angle θ_d.

The masonry infills are also modeled with truss assemblages, as schematically summarized in Fig. 2. More specifically, each brick is modeled with two truss cells. The truss geometry is determined from the dimensions of the bricks. The spacing of the vertical elements is equal to $0.5L_b$, where L_b is the length of a brick unit, and the spacing of the horizontal truss elements is equal to the height, H_b, of the brick. Knowledge of the horizontal and vertical dimensions of the truss cell allows to uniquely determine the inclination angle, θ_d, of the diagonal truss elements of the cells. Ultimately, each masonry unit is represented with three vertical, four horizontal and four inclined truss elements.

The mortar joints and infill-to-frame interfaces must also be accounted for in the analyses, since they constitute weak planes where localized mode-I (tensile) opening and/or shear sliding can occur. Additionally, it is necessary to capture the contact stress distribution along the infill-to-frame interface with adequate accuracy. To describe these aspects of behavior, the proposed modeling scheme relies on zero-length macroelements, i.e. assemblages of several nonlinear spring elements, at the locations of the mortar interfaces (e.g., bed and head joints), as shown in Fig. 2. These elements are described in detail later in the paper.

The determination of the truss geometry is completed by establishing the cross-sectional areas of the various elements. In accordance with the approach in Panagiotou et al. [40], the cross-sectional area of each element is obtained as the product of a tributary sectional width times the out-of-plane thickness of the masonry wall. For the vertical elements, a distinction is made between the two external elements and the intermediate element of the truss representation of a unit. For an infill wall with thickness t, the cross-sectional areas of the external elements, $A_{v,ext}$, and of the intermediate element, $A_{v,int}$, are given by the following equations.

$$A_{v,ext} = 0.25L_b \cdot t \tag{1}$$

$$A_{v,int} = 0.5L_b \cdot t \tag{2}$$

The cross-sectional area A_h of the horizontal truss elements is given by the following expression.

$$A_h = 0.5H_b \cdot t \tag{3}$$

Finally, the following equation provides the cross-sectional area of the diagonal elements.

$$A_d = b_{eff} \cdot t \tag{4}$$

where the tributary width, b_{eff}, of these elements is obtained from an equation proposed in Panagiotou et al. [40]:

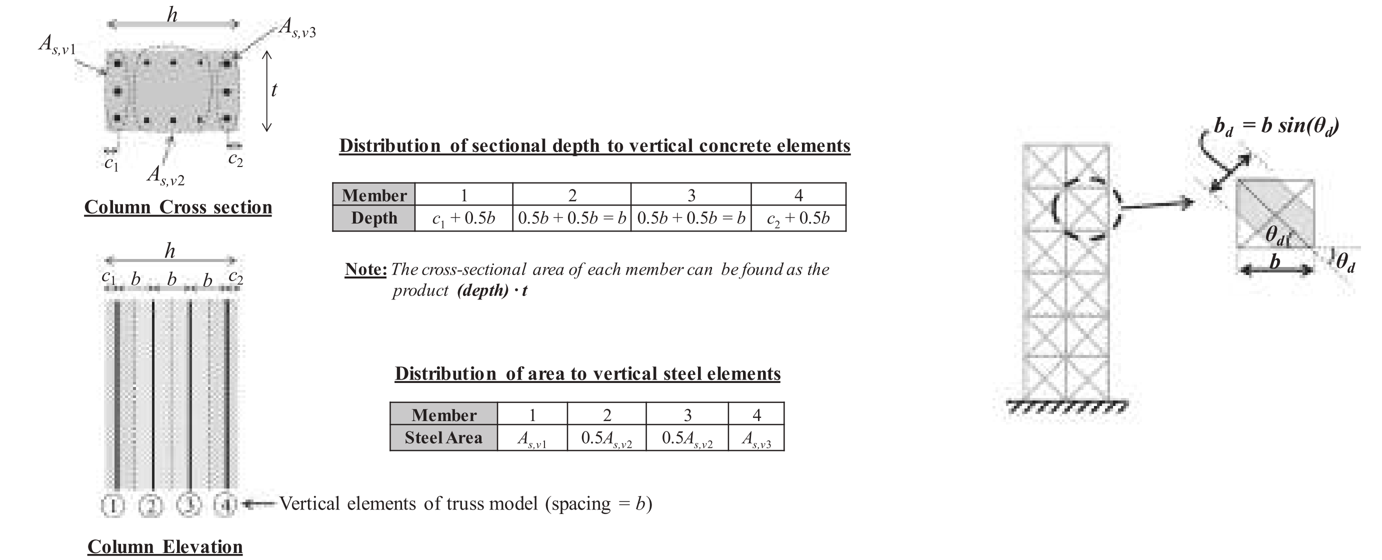

Fig. 1. Modeling approach for RC columns (figure from [38].

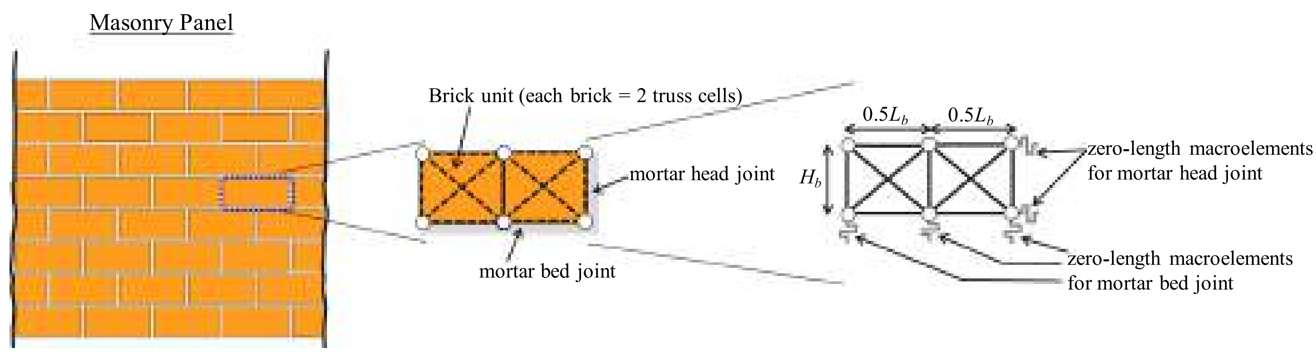

Fig. 2. Modeling Approach for Brick Masonry Infill Walls.

$$b_{eff} = 0.5L_b \cdot \sin(\theta_d) \tag{5}$$

2.1. Material models for truss elements

The truss elements are provided with constitutive models to capture the nonlinear material response of concrete, masonry and steel reinforcement. The material model for concrete and masonry, which is schematically summarized in Fig. 3a, is the one formulated by Lu and Panagiotou [30]. This model can capture the strength and stiffness degradation due to cracking and the compressive strength degradation due to crushing. This constitutive law can also account for the effect of transverse tension on the compressive resistance of the diagonal truss

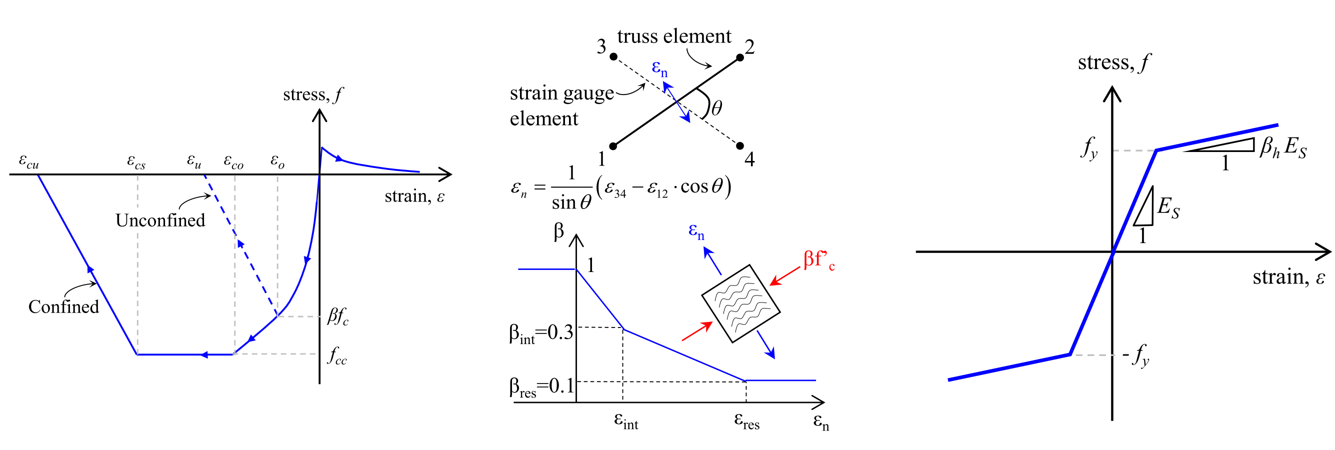

(a) Stress-strain law for concrete and masonry (b) Calculation of transverse strain (c) Stress-strain law for steel

Fig. 3. Constitutive models for concrete, masonry and reinforcing steel.

elements. To this end, an additional pair or nodes needs to be defined for each diagonal element, to provide a "strain gauge element" for the computation of the transverse strain as shown in Fig. 3b. The transverse strain allows the calculation of a reduction coefficient, β, that is used to adjust the compressive stresses of the diagonal elements and varies with the transverse strain. A special truss element formulation, termed *Truss2* and allowing the definition of the additional pair of nodes for measuring the transverse strain at each step of an analysis, is available in *OpenSees*.

To prevent the occurrence of spurious mesh size effects due to strain localization [5,11,40,30], the softening portion of the constitutive law for tension and compression is regularized, i.e. adjusted with element size. In the present study, the regularization is based on the assumption that the reference stress–strain laws which are defined correspond to an element size of 600 mm (23.62 in). This value is based on the length over which average strains were measured in the concrete panel tests by Vecchio and Collins [54].

The behavior of the reinforcing steel is described by means of the Giuffre-Menegotto-Pinto (GMP) model [16], which is implemented in *OpenSees* and schematically summarized in Fig. 3c. The GMP model is characterized by a monotonic envelope curve with linear hardening after yielding. Since bar buckling and rupture did not occur in the analysis cases considered herein, they are not accounted for in the present study.

2.2. Zero-length macroelements to account for the effect of mortar joints

The zero-length macroelements used for the mortar joints and infill-to-frame interfaces, schematically summarized in Fig. 4, are capable of accounting for the normal tensile opening and closing, shear fracture and frictional shear sliding. These elements develop two stress components with respect to the plane of a mortar interface, namely, a normal stress component, σ, and a shear stress component, τ. The stress components of the macroelement are obtained as the sum of the stresses contributed by individual spring elements which are used to account for different aspects of the mortar interface behavior, as explained below.

First, a nonlinear spring element which can only develop tensile resistance is included in the normal direction, to describe normal crack opening and tensile strength degradation. The latter is described by an elastic-softening law, which consists of three linear segments. A similar nonlinear spring with linear isotropic softening is aligned with the shear direction of the interface, to describe cohesive shear (Mode-II) fracture. Finally, a shear-sliding spring is used to account for the frictional-sliding-shear resistance and for the normal compressive behavior of the interface. This spring behaves as an elastic gap element in the normal direction. Specifically, it has a linearly elastic behavior for compressive deformation, while it does not develop any resistance for tensile (opening) deformation. The spring also has a Coulomb elastoplastic behavior in the shear direction, wherein the yield strength is linearly proportional to the normal compressive force of the spring. If the normal force is tensile or zero, then the shear-sliding spring develops no shear (sliding) resistance. This type of Coulomb-frictional spring behavior can be obtained through use of the flat slider element in *OpenSees* [47]. At

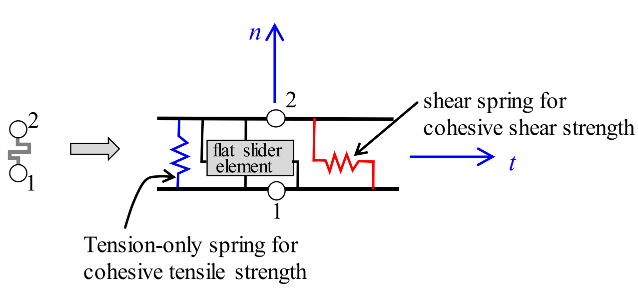

Fig. 4. Zero-length macroelement for capturing localized damage on mortar joints.

each step in an analysis, the normal stress, σ, and the shear stress, τ, of the interface are the sum of the corresponding spring contributions. Thus, the following relations can be established.

$$\sigma = \sigma_c + \sigma_s \tag{6}$$

$$\tau = \tau_c + \tau_s \tag{7}$$

In Eqs. (6) and (7), the subscript 'c' denotes the contribution of a cohesive spring, while the subscript 's' denotes the contribution of the frictional spring. The individual contributions of the different spring elements to the normal and shear stress are schematically summarized in Figs. 5a and 5b, respectively.

The softening laws of the nonlinear springs must comply with fracture mechanics-based concepts. Specifically, the area under the softening portion of the stress-displacement law in the tension-only, cohesive normal spring is equal to the mode-I fracture energy, G_f^I , of the interface, as shown in Fig. 5a. This value can be determined from experimental tests. For example, tests by Pluijm [42] yielded a value of G_f^I ranging from 0.005 to 0.02 [N.mm/mm^2]. Similarly, the area under the stress-displacement curve corresponding to the elastic-softening cohesive shear spring of Fig. 5b is equal to the mode –II fracture energy,G_f^{II}, of the interface. The value of G_f^{II} is typically set equal to about 10 times that of G_f^I [50,23].

The force in the nonlinear springs that comprise the zero-length macroelements is obtained by multiplying the stress values by a spring sectional area. Figure 6 presents an element assemblage taken from the truss model of an infill wall. In the actual truss model, any two nodes that are interconnected by a macroelement are coincident, i.e. they occupy the same exact location in space. To enhance the clarity of the figure, the macroelements are shown with a nonzero length. Figure 6 indicates that each head joint corresponds to two macroelements, while each truss cell corresponds to two macroelements representing bed joints. These observations lead to the conclusion that the area of the springs corresponding to mortar bed joints should be equal to the sectional area $A_{v,ext}$ of the external vertical truss elements, given by Eq. (1), while the area of the springs corresponding to the head joints should be equal to the sectional area A_h of the horizontal truss elements, obtained from Eq. (3).

The macroelements also require the calibration of interface stiffness parameters. The stiffness of the springs representing normal behavior in Fig. 5a and of the elastic-softening shear spring in Fig. 5b is assigned the same value, K, which is essentially a penalty stiffness parameter. A different value of stiffness K_f, is assigned to the Coulomb-frictional law of the shear-sliding spring shown in Fig. 5b.

2.3. Preliminary verification of capability of zero-length macroelements to capture behavior of interfaces

A set of preliminary analyses is conducted to verify the capability of the macroelements to capture the salient features of interface response. The verification is based on a comparison of the results obtained using the proposed macroelement and those obtained with the cohesive-crack interface element by Lourenço and Rots [29], which is available in the finite element analysis software DIANA [53]. The truss and finite element model are both calibrated using the interface parameter values shown in Table 1. The loading is conducted for a set of two brick units, with a mortar bed joint in-between, as shown in Fig. 7a. This physical system is analyzed with both the approach proposed herein, and with a combination of quadrilateral solid elements for the units and a zero-length interface element for the mortar joint. To allow a direct comparison of the mortar interface behavior for the two modeling approaches, the boundary conditions in the analyses are such that deformation can only occur at the mortar joint interface.

A first verification analysis is conducted for the case of mode-I fracture, i.e., normal tensile opening, of the mortar interface. The

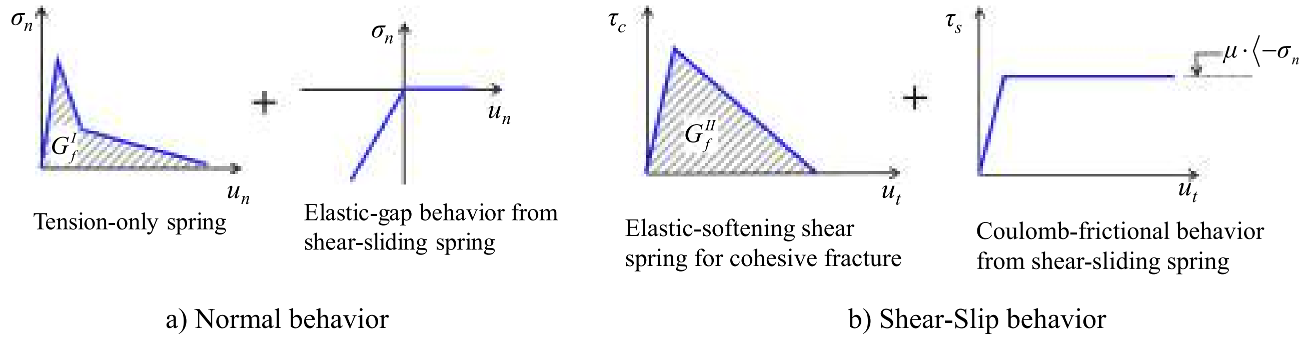

Fig. 5. Stress-displacement behavior of various components comprising the zero-length macroelement.

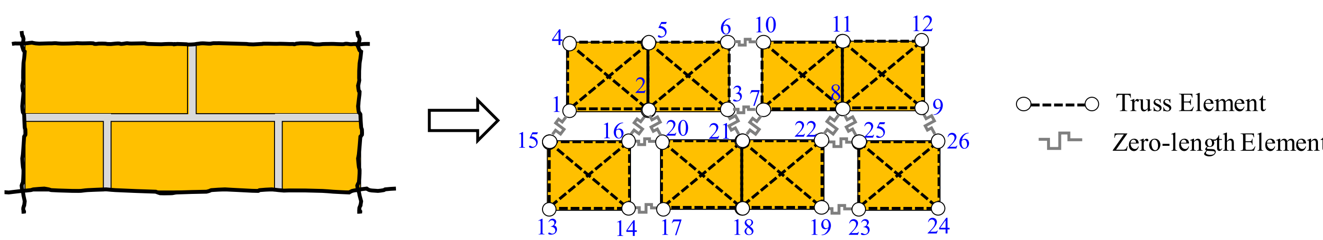

Fig. 6. Example mesh connectivity for representing the mortar bed and head joints in an infill wall.

Table 1
Material properties used in the interface verification analysis.

f_t (kPa)	G_f^I (kPa-mm)	C (kPa)	G_f^{II} (kPa-mm)	μ	K (kN/mm)	K_s (kN/mm)
276	88	412	5314	0.85	700	32

comparison of the obtained plots of tensile stress as a function of crack opening displacement in Fig. 8 indicates that the model can capture the tensile strength degradation due to mode-I crack opening. The minor discrepancy between the truss model and the finite element model is due to the fact that the softening law is described by straight-line segments in the former and by an exponential smooth curve in the latter.

An additional verification analysis is conducted for Mode-II fracture and frictional-shear sliding along the mortar joint interface under a constant, normal compressive stress of 705 kPa, as shown in Fig. 9a. As shown in Fig. 9b, the interface develops a relatively large shear stiffness, up to the point where the shear stress reaches the initial shear-sliding capacity. The latter expresses the combined effect of Coulomb frictional resistance and cohesive shear strength. After the initial shear-sliding strength is reached, a degradation of the shear strength is observed with increasing shear-sliding displacement, up to the point where a constant, residual capacity is attained. The latter is simply equal to the product of the frictional coefficient times the magnitude of the normal compressive stress.

To elucidate the contribution of the various components to the shear resistance of the zero-length macroelement, Fig. 9c provides the evolution of the resistance of the cohesive-shear spring and of the shear-sliding spring. As expected, both of these components have a large penalty stiffness, and reach their peak capacity for a very low value of sliding displacement. While the resistance of the sliding spring remains constant with increasing sliding displacement, that of the cohesive spring degrades until it becomes practically equal to zero. Thus, the shear strength degradation of the macroelement shown in Fig. 9b is caused by the loss of the resistance of the cohesive-shear spring.

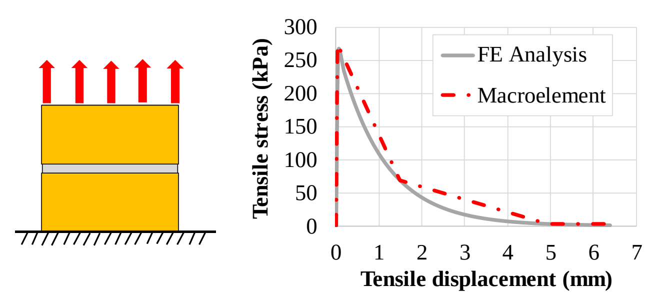

Fig. 8. Preliminary verification analysis for normal tension (Mode-I fracture).

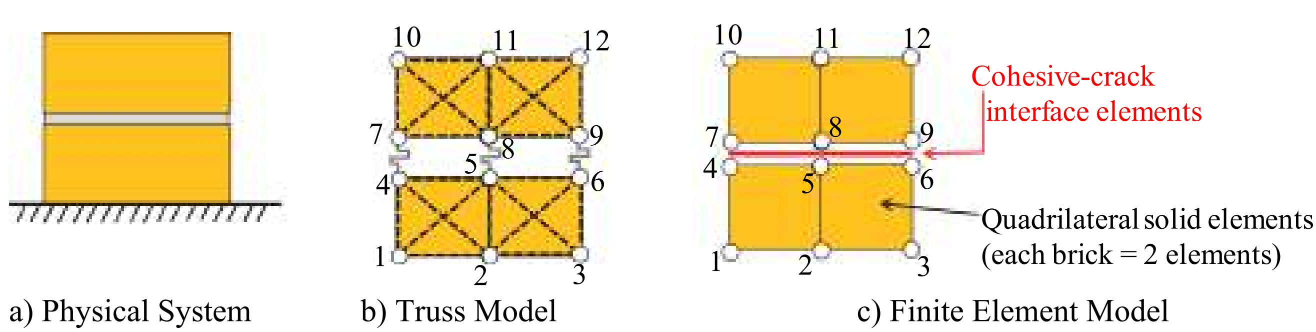

Fig. 7. Case study for preliminary verification of capability of zero-length macroelements to capture the behavior of mortar joints.

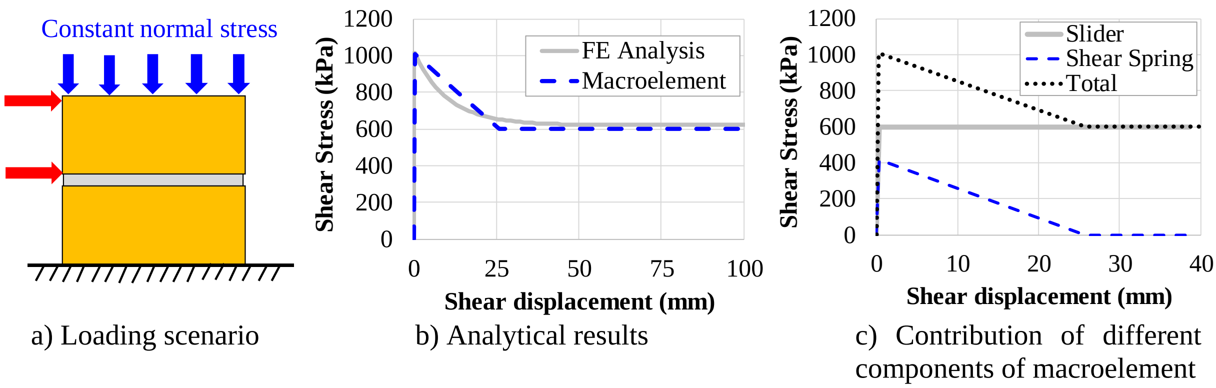

Fig. 9. Preliminary verification analysis for shear loading (Mode-II fracture and shear sliding).

3. Validation of truss modeling approach for infilled frames

The truss modeling approach is validated using the results of experimental tests by Mehrabi et al. [36]. The validation study is focused on three specimens, which were subjected to monotonic lateral loads until the occurrence of severe damage. The first specimen was a bare RC frame, the second specimen included a relatively weak infill wall made of hollow units, and the third specimen included a relatively strong infill wall that consisted of solid units. The height-to-length ratio of the infill walls was equal to 0.67. The three specimens constituted parts of a prototype RC frame structure, which was not designed for ductile seismic response. The longitudinal reinforcement in the columns consisted of eight No. 4 bars with a diameter of 13 mm, while that in the beams consisted of four No. 5 bars (two at the top of the section and another two at the bottom), with a diameter equal to 16 mm. The transverse reinforcement consisted of No. 2 bars (having a diameter of 6 mm) spaced at 63 mm (2½ inches) and at 76 mm (3 in.) for the columns and beams, respectively. A constant vertical load was applied to each specimen. For the two infilled specimens, 33% of the vertical load was applied on the beam, and the remainder of the load was applied on the columns. The specimen configuration is shown in Fig. 10. The same RC frame was used for all specimens. After the completion of each of the first two tests, the frame was repaired by application of epoxy injections in the cracked regions and patching up the crushed regions with cement paste of strength comparable to that of the original concrete [36]. The salient parameters of the three specimens are summarized in Table 2.

To ensure that the validation analyses are not limited to a single study from the literature, the modeling scheme has also employed for simulation of specimen S2H tested by Fiorato [17]. The single-story, single-bay specimen included a brick infill wall with no openings, and constituted a 1/8-scale version of a prototype frame. The frame columns had a square cross-section with a dimension of 76 mm (3 in.), while the frame beam had a sectional depth of 152 mm (6 in.). Each column had eight longitudinal round bars with a diameter of 4.5 mm, corresponding to a reinforcement ratio of 2.2%. Each column contained a single closed stirrup, located at mid-height. The single-wythe infill wall had a thickness of 22 mm (0.875 in.).

Table 2
Test Specimens by Mehrabi et al. [36] considered in validation analyses.

Specimen	Type of Masonry Units	Panel Aspect Ratio (h/L)	Vertical Load Distribution (kN)	
			Columns (P_1)	Beam (P_2)
1	No infill	0.67	146.85	–
8	Hollow		97.90	48.95
9	Solid		97.90	48.95

The parameters of the constitutive models for the truss elements are assigned the values presented in Table 3. The corresponding parameters for the zero-length macroelements are provided in Table 4. For the specimens tested by Mehrabi et al. [36], the uniaxial compressive strength, modulus of elasticity, and compressive strain corresponding to the peak compressive stress for both concrete and masonry have been set equal to the values obtained from material tests accompanying the experimental study. The same applies for the yield stress of the reinforcing steel. Fiorato [17] provided values for the uniaxial compressive strength and modulus of elasticity of the concrete, and for the yield

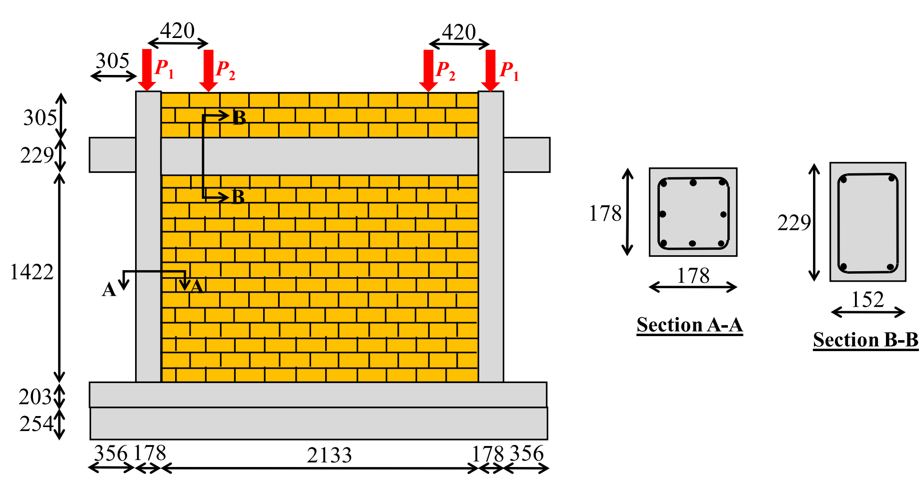

Fig. 10. Configuration of infilled frame specimens for validation analysis (dimensions in mm).

Table 3
Material Parameter Values in Truss Elements Used in the Analyses of Infilled Frames.

Material element	Concrete/Masonry								Steel				
	$f_c^{'}$ (MPa)	ε_o	f_t (MPa)	E_c (MPa)	$A_{v,ext}$ (cm^2)	$A_{v,int}$ (cm^2)	A_h (cm^2)	A_d (cm^2)	$A_{sl,ext}$ (cm^2)	$A_{sl,int}$ (cm^2)	A_{st} (cm^2)	f_{yl} (MPa)	f_{yt} (MPa)
RC Frame by Mehrabi et al. [36]													
columns	26.8	0.0027	2.7	19,676	92.6	131.0	181	106.1	3.9	2.6	1.0	421	368
beam					77.4	154.8	151	108.1	0.8	0.8	4.0		
RC Frame by Fiorato [17]													
columns	31.	0.0038	3.1	16,506	19.9	18.2	13.8	11.0	0.66	0.00	0.005	292	292
beam					22.6	23.6	29.0	18.3	0.63	0.63	0.009		
Infill Wall with Hollow Units [36]													
	9.5	0.0027	1.0	6980	23.2	46.5	23.2	32.8	n.a.				
Infill Wall with Solid Units [36]													
	14.2	0.0026	1.4	10,420	46.8	93.5	46.8	66.1	n.a.				
Infill Wall [17]													
	26.5	0.0035	2.7	15,169	3.4	6.8	1.6	2.9	n.a.				

Note: $f_c^{'}$ is the uniaxial compressive strength, ε_o is the compressive strain corresponding to the peak compressive stress (for uniaxial compression), f_t is the tensile strength, E_c is initial modulus of elasticity, $A_{v,ext}$ is the cross-sectional area of the longitudinal truss elements at the ends of the section, $A_{v,int}$ is the cross-sectional area of the intermediate longitudinal truss elements, A_h is the cross-sectional area of the transverse truss elements for a member (horizontal elements for columns and infill walls, vertical elements for beams), A_d is the cross-sectional area of the inclined truss elements, $A_{sl,ext}$ is the cross-sectional area of the longitudinal reinforcement truss elements at the ends of the section, $A_{sl,int}$ is the cross-sectional area of the intermediate longitudinal reinforcement truss elements, A_{st} is the cross-sectional area of the transverse reinforcement truss elements for a member. Finally, f_{yl} and f_{yt} are the yield stress of the longitudinal and transverse reinforcement, respectively.

Table 4
Parameter Values in Zero-Length Macroelements Used in the Analyses of Infilled Frames.

f_t (kPa)	G_f^I (kPa-mm)	C (kPa)	G_f^{II} (kPa-mm)	K (kN/mm)	K_s (kN/mm)	μ
Specimen by Mehrabi et al. [36] **with Weak Infill Wall**						
283	66	283	660	700	32	0.75
Specimen by Mehrabi et al. [36] **with Strong Infill Wall**						
538	66	538	660	700	32	0.75
Specimen by Fiorato [17]						
159	77	159	770	700	32	0.75

stress of the reinforcing steel. The masonry material parameters had to be assumed for this specimen, as masonry prism test data was not provided.

The tensile strength of the concrete and of the masonry units is set equal to 10% of the corresponding uniaxial compressive strength. The experimental studies were not accompanied with material tests for the mortar joints. For this reason, the calibration of the zero-length macroelement strength and fracture energy parameters was based on recommendations by Al-Chaar et al. [2], Stavridis and Shing [50] and Koutromanos et al. [26] for the corresponding calibration of cohesive-crack interface elements. The stiffness parameters of the macroelements are set to a value which is sufficiently high to warrant accurate results, while avoiding potential occurrence of convergence difficulties in the analyses.

3.1. Analysis of bare RC frame

The first analysis using the truss modeling approach is conducted for a bare RC frame, which was labelled Specimen 1 in Mehrabi et al. [36]. The specific frame was flexure-dominated, and it exhibited a ductile response mechanism with inelastic flexural deformations in the columns. The deformed shape of the truss model at a drift ratio of 2.5% is presented in Fig. 11a, while Fig. 11b provides a comparison of the load–displacement response with the corresponding experimental observations. The truss model can accurately capture the strength of the specimen, but it overestimates the pre-peak stiffness. This is due to the fact that the effect of the bond-slip deformations at the column ends is not accounted for in the model. The analysis for the frame has been repeated, this time accounting for the additional deformations at the column ends due to strain penetration. The procedure by Moharrrami et al. (2015) to account for strain penetration deformations in truss models of RC columns is employed. As shown in Fig. 11b, the incorporation of the strain penetration effect significantly improves the analytical estimate of the pre-peak stiffness of the bare frame. As explained in Mehrabi et al. [35], the bond-slip effect is significant for the response of bare frames, but insignificant for the response of infilled frames. For this reason, the strain penetration effect is not considered in the remainder of the present study.

3.2. Analysis of Masonry-Infilled RC frames

The next validation analysis is conducted for two infilled specimens, labelled as Specimens 8 and 9, respectively, in Mehrabi et al. [36]. Specimen 8 included a relatively weak infill wall consisting of hollow masonry units and exhibited a relatively ductile response, with fairly distributed damage along the height of the infill wall. Specimen 9 had a relatively strong infill wall made of solid units and the damage pattern was dominated by the formation of diagonal-sliding cracks in the infill wall and a subsequent shear crack at the top of the windward column. The comparison between the analytically obtained and the experimentally recorded load–displacement curves, provided in Fig. 12a for Specimen 8 and Fig. 12b for Specimen 9, indicates that the analytical models provide satisfactory estimates of the response for both cases. The peak strength is underestimated by 3.5% in the analysis of Specimen 8 and overestimated by the same amount in the analysis of Specimen 9. The only significant discrepancy is observed in the analysis of Specimen 9, where a significant degradation in capacity occurs at a drift ratio of 2.06%, as shown in Fig. 12b. An explanation for this degradation in the analysis will be provided after a presentation of the analytically obtained damage patterns and response mechanisms.

The analytical models provide insights on the deformation modes and the damage pattern evolution for the case of a weak infill and a strong infill. The deformations in the infill wall for Specimen 8 are fairly uniformly distributed along the height, as deduced from the contour plots shown in Fig. 13a and 13b, for drift ratios of 0.2% and 2.5%, respectively. The plot of Fig. 13b also indicates sliding along several bed joints over the height of the specimen, which was also the case in the experimental test. Such sliding is manifested as a discontinuity of the contour plot value across a plane consisting of multiple zero-length macroelements. The analysis of Specimen 9 gives a fairly uniform distribution of deformations in the infill at early stages of response. In fact,

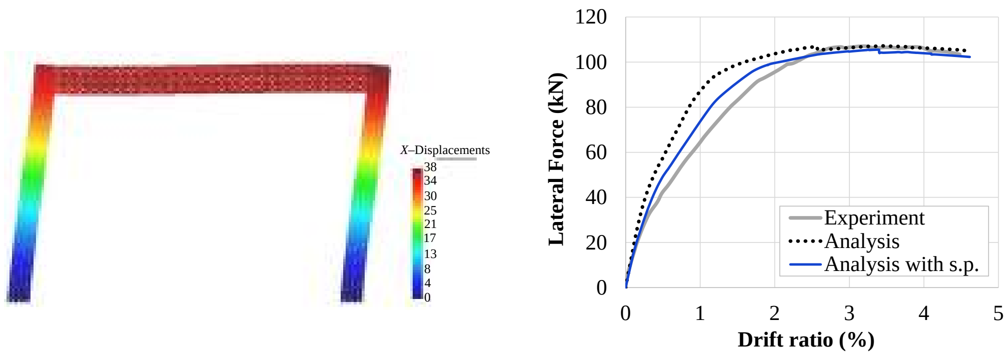

a) Deformed shape and horizontal displacement contour (in mm), at a drift ratio of 2.5%.

b) Load-displacement response and effect of accounting for strain penetration (s.p.) in the analysis.

Fig. 11. Results of nonlinear static analysis for bare frame specimen tested by Mehrabi et al. [36].

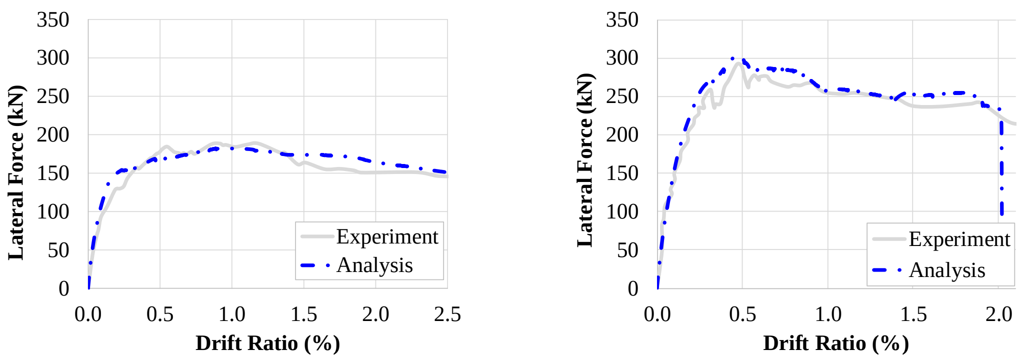

a) Specimen with weak infill wall

b) Specimen with strong infill wall

Fig. 12. Comparison of analytically obtained and experimentally recorded load–displacement response for infilled frame specimens tested by Mehrabi et al. [36].

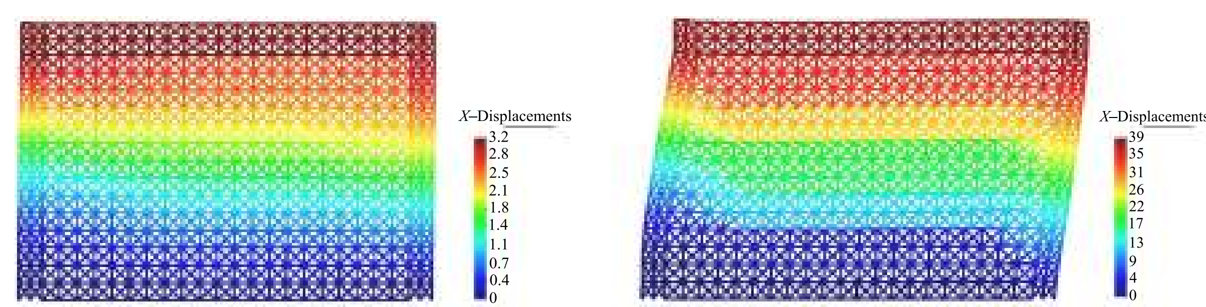

a) Specimen with weak infill, drift ratio of 0.2%.

b) Specimen with weak infill, drift ratio of 2.5%

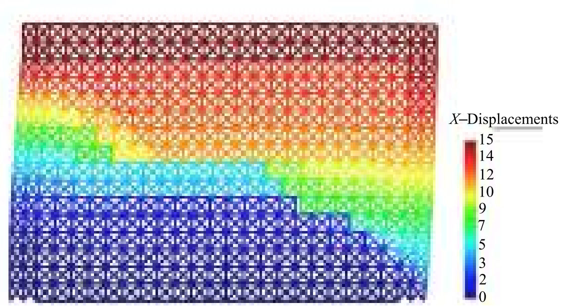

c) Specimen with strong infill, drift ratio of 0.5%

Fig. 13. Deformed shape (deformations magnified by a factor of 5) and horizontal displacement contours (in mm) for infilled frame specimens tested by Mehrabi et al. [36].

the horizontal displacement contour plot at a drift ratio of 0.2% is practically identical to the one shown in Fig. 13a for Specimen 8. For larger lateral deformations, the deformation distribution in the infill wall significantly changes. As shown in Fig. 13c, the horizontal displacement contour plot for a drift ratio of 0.5% indicates the formation of a diagonal-horizontal sliding crack pattern in the infill wall, which is manifested through a visible discontinuity in the contour color distribution. Additional deformations are concentrated across the specific infill crack with further loading.

The strain contours of the truss elements corresponding to the frame members provide insights on the analytically predicted damage of the RC frames. Large tensile strains in the vertical truss elements of the columns would be associated with flexural cracking. On the other hand, large tensile strains in the horizontal and diagonal truss elements of the columns would be indicative of shear cracking and failure. The strain contours for the RC frame of Specimen 8, presented in Figs. 14a-d for drift ratios of 0.2%, 0.5%, 1.0% and 2.0%, respectively, indicate that the damage in the frame was associated with a flexure-dominated response, since the strains are fairly distributed along the column height and the maximum strains are obtained at the vertical members in the vicinity of the column ends. As expected, the strain values in these regions increase for increasing levels of lateral deformation in the specimen. The frame behavior for Specimen 9 at low levels of lateral drift is similar to that of Specimen 8. Accordingly, the strain contour plots at drift ratios of 0.2% and 0.5% are very similar to those presented in Figs. 14a and 14b, respectively, for Specimen 8. At larger values of drift, the formation of the diagonal-sliding crack in the infill wall of Specimen 9 leads to the development of large shear forces at the top of the windward column and at the bottom region of the leeward column. These forces cause shear-related damage to occur in these column regions, as deduced from the contour plots for drift ratios of 1.0% and 2.0%, shown in Figs. 15a and 15b, respectively. The shear damage is indicated by the relatively large tensile strains (in excess of 1%) in the diagonal truss elements at the top of the windward column, and by the large tensile strains in horizontal elements at the bottom of the leeward column. Although the shear damage in the experimental test was more pronounced in the windward column, the model gives significant damage of this type in the leeward column as well.

A comparison of the deformed shape at the end of the analysis for Specimen 8 to the corresponding experimental observation is provided in Fig. 16. The sliding and opening deformations of the spring elements representing the mortar joint interfaces allow to deduce the main cracks in the infill wall, marked in red color in Fig. 16b. The occurrence of distributed sliding cracks along the height of the infill wall and the absence of localized shear distortions in the frame members are evident in the analytical deformed shape. A similar comparison between the deformed shape at the end of the analysis for Specimen 9 with the experimental cracking pattern is presented in Fig. 17. The analytical model gives a strongly localized shear damage at the windward column, as marked in Fig. 17b, which leads to a lateral strength degradation of the specimen. As mentioned above, the analysis for this specimen predicted a very sudden, significant strength degradation at a drift ratio of about 2%, which was not present in the experimental test. This fact is attributed to the dowel action of the reinforcing steel, which is expected to have had a contribution to the resistance of the open shear crack and was not accounted for in the model. Still, this disagreement may not be deemed significant, since it occurs at a very late stage of the analysis. The cracking pattern in the infill is also a satisfactory reproduction of the experimentally recorded one, which consisted of a combination of diagonal and sliding cracks. It is worth mentioning that the results obtained herein are of comparable – if not better – accuracy than those obtained in other studies (e.g., [2,50]) with much more refined and complicated, nonlinear finite element models.

Figures 18a and 18b present contour plots of the compressive stresses in the truss elements used for the infill walls of Specimens 8 and 9, respectively, obtained at the instant of peak lateral resistance in the analyses. These contour plots enable to infer the presence of inclined banded regions with compressive stresses, mimicking the formation of struts in the infills. Interestingly, none of the two figures indicates the formation of a single-strut resistance mechanism in the infill wall. This observation, which is similar to results presented for refined finite element analyses of infilled frames in Chapter 5 of Stavridis [49], would indicate that a simple, equivalent-strut model would probably not be capable of accurately reproducing the resistance mechanism of the two infilled frames.

The analytically obtained load–displacement response of the

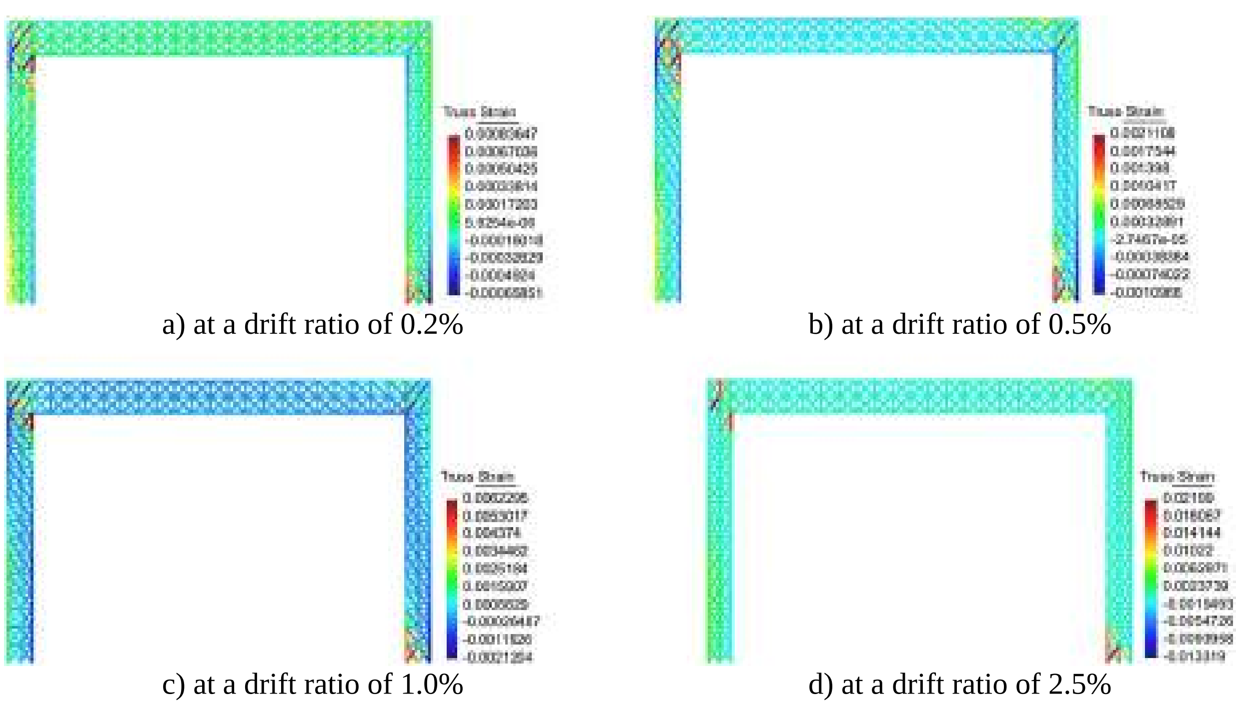

Fig. 14. Strain contours in frame members for specimen with weak infill wall tested by Mehrabi et al. [36].

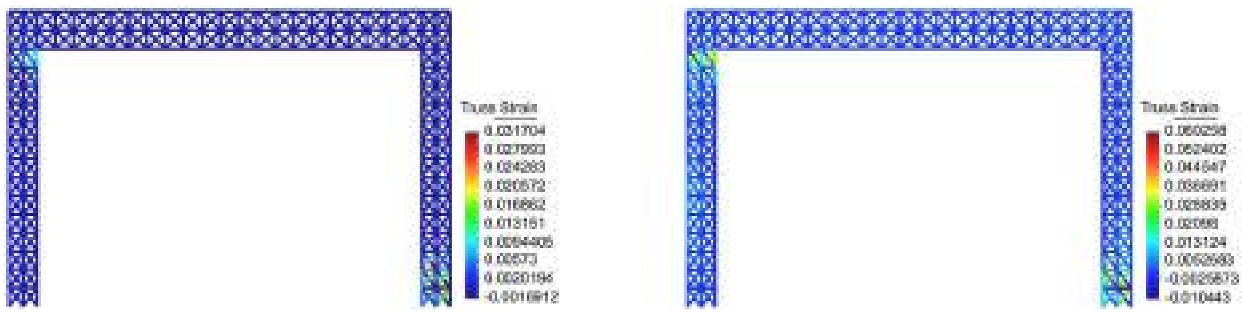

a) at a drift ratio of 1% b) at a drift ratio of 2%

Fig. 15. Strain contours for specimen with strong infill wall tested by Mehrabi et al. [36].

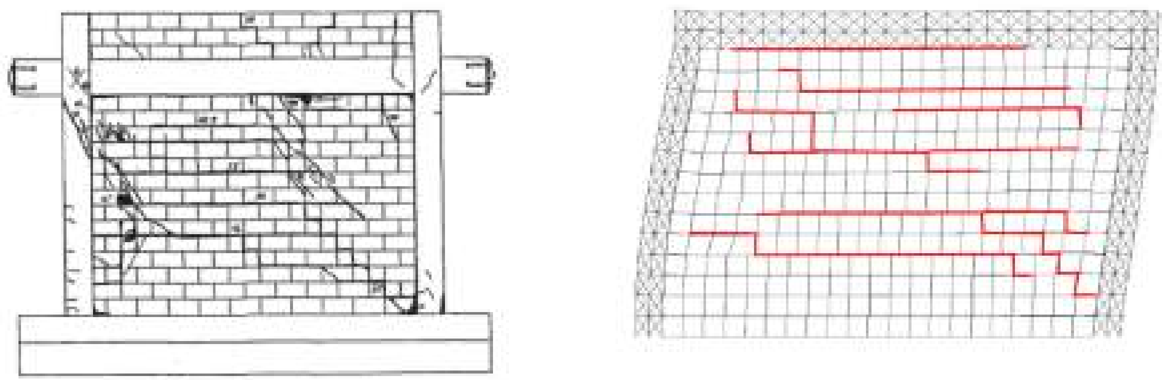

a) Experimentally observed damage pattern at end of test

b) Damage pattern in infill wall at end of analysis (diagonal truss elements in infill not shown for clarity)

Fig. 16. Damage pattern for specimen with weak infill wall tested by Mehrabi et al. [36].

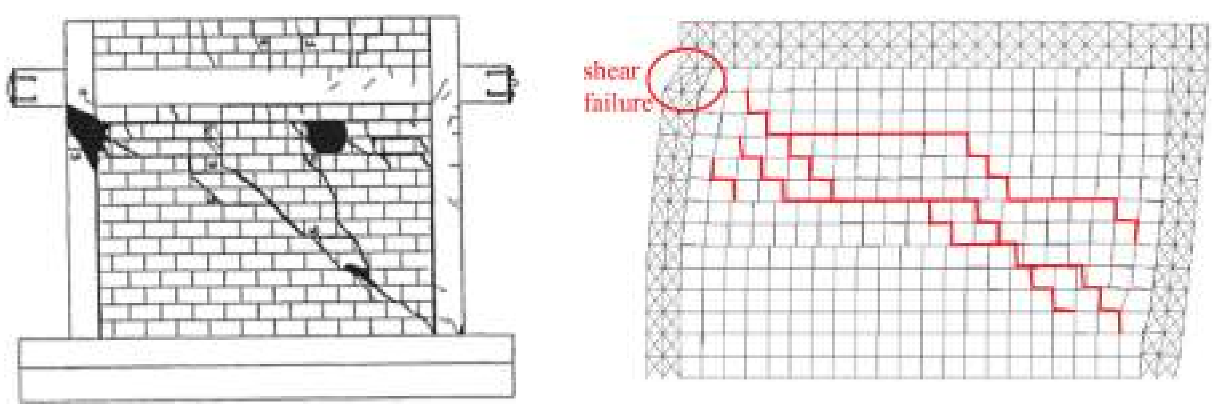

a) Damage pattern at end of test.

b) Damage pattern at end of analysis (diagonal truss elements in infill not shown for clarity)

Fig. 17. Damage pattern for specimen with strong infill wall tested by Mehrabi et al. [36].

specimen by Fiorato [17] is compared to the corresponding experimental data in Fig. 19a. The comparison of the crack pattern at the end of the test to the corresponding deformed finite element mesh is provided in Fig. 19b. Overall, the analysis can satisfactorily reproduce the response of the specimen, including the peak strength, post-peak force-displacement response, and the damage pattern, which primarily consisted of horizontal sliding cracks in the mortar bed joints of the upper half part of the infill wall height.

3.3. Sensitivity analysis for mortar interface parameters

The analysis of an infilled frame requires the calibration of the material parameters for the truss model and for the zero-length macroelements which represent the mortar-joint interfaces. While the mortar

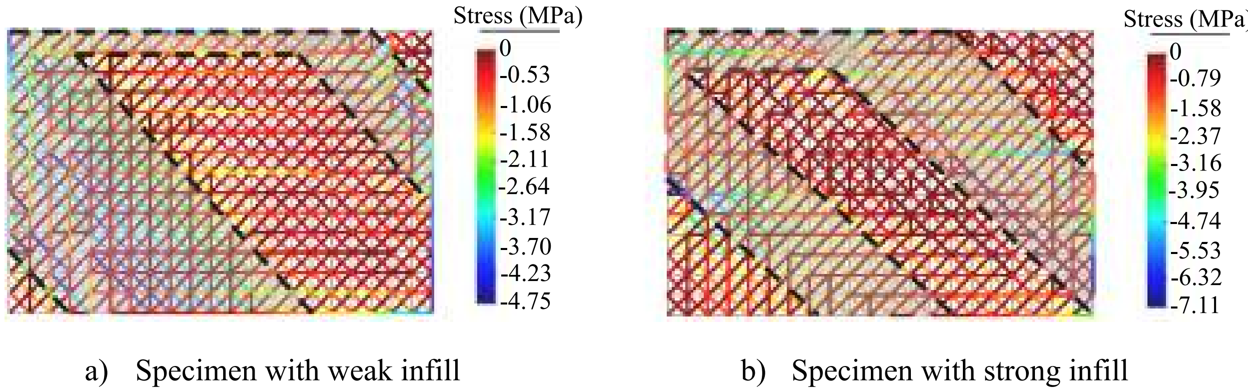

Fig. 18. Compressive stress contours in truss elements representing infill walls at the maximum lateral resistance for the two infilled frame specimens tested by Mehrabi et al. [36].

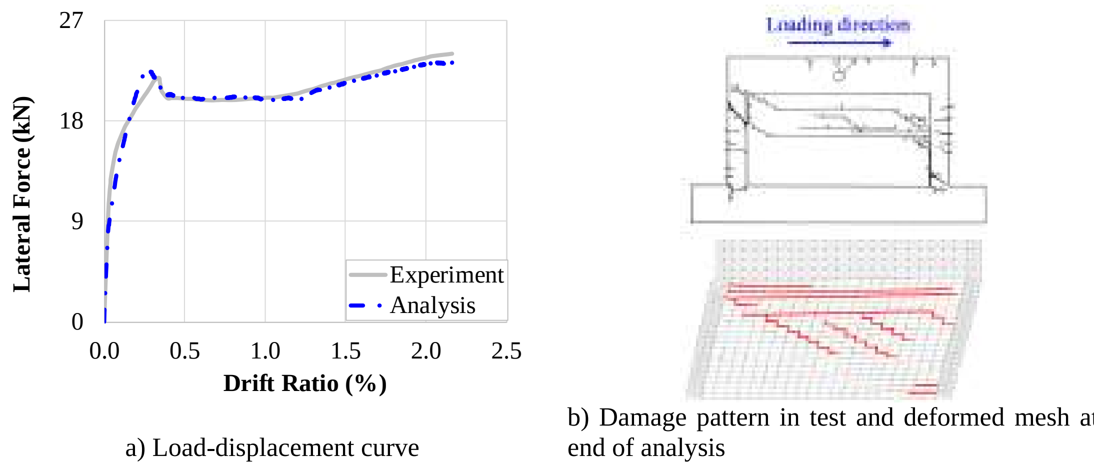

Fig. 19. Results of validation analysis for infilled frame specimen tested by Fiorato [17].

joint material properties can be determined from experimental tests such as bond-wrench and triplet tests, test data may not always be available. Consequently, the value of the cohesive and frictional strength of the mortar interfaces in an analysis may be characterized by greater uncertainty than, e.g., the concrete or reinforcing steel material parameters. To elucidate the effect of the interface parameters on the analytically obtained nonlinear response of infilled RC frames, this section presents a sensitivity study for the parameters of the zero-length macroelements.

The sensitivity study relies on multiple repetitions of the analysis for Specimen 9 by Mehrabi et al. [36]. In each repetition, the value of a material parameter is varied, while the remaining parameters have the same values as those used in the analysis of Section 3.2. This latter analysis is treated as the baseline case. The load–displacement curves obtained for different values of the tensile strength, mode-I fracture energy, sliding-shear stiffness and frictional coefficient of the interface, are presented in Figs. 20a, 20b, 20c, and 20d, respectively. The tensile strength, fracture energy, sliding stiffness and frictional coefficient are expressed in terms of the respective quantities f_{t0},G^{I}_{f0}, K_{f0} and μ_0 used in the baseline case. The range of values for modeling parameters f_t, G^{I}_{f} and μ was selected to reflect the values of these interface parameters adopted in the literature [2,50,26]. On the other hand, a wider range of values has been considered for the stiffness parameter K_s. The reason is that the specific parameter affects a penalty stiffness (not a physical stiffness), which is why it was deemed necessary to consider values of K_s ranging from 50% of the value adopted in the validation analyses to 400% of that same value.

To quantify the effect of different parameters on the analytical results, the sensitivity is expressed in terms of three response quantities, namely, the peak lateral strength, the drift ratio corresponding to the peak lateral strength, and the inelastic deformability. The latter is expressed through the drift ratio corresponding to a lateral resistance degradation of 15%. The sensitivity of these quantities is summarized in Figs. 21 and 22. In the specific figures, the value obtained for each analysis case is divided by the corresponding value of the baseline case.

Based on the data presented in Fig. 21a, the peak strength is more sensitive to the strength parameters of the zero-length macroelements, namely, the tensile resistance and the frictional coefficient. An increase in either of these two parameters leads to an increase in the peak strength of the infilled frame. Increasing the frictional coefficient by 20% leads to a very strong infill wall, while also limiting the sliding along the infill-to-frame horizontal interface. This ultimately leads to a damage pattern that involves the occurrence of a shear failure in the frame column at a relatively low level of lateral displacement, entailing a significant strength degradation, as attested by the corresponding load–displacement curve in Fig. 20d. Still, the specific case corresponds to a rather unrealistic mortar interface sliding strength (i.e., a constant frictional coefficient equal to 0.9), which may be overly high for mortar joints. The mode-I fracture energy of the cohesive elements is also found to affect the strength, although its effect is less pronounced than that of the strength parameters. The sliding-shear stiffness value for the zero-length macroelements is found to have a relatively minor effect on the strength.

The value of drift ratio at peak strength is more sensitive to the parameters considered, as deduced from Fig. 21b. The strength

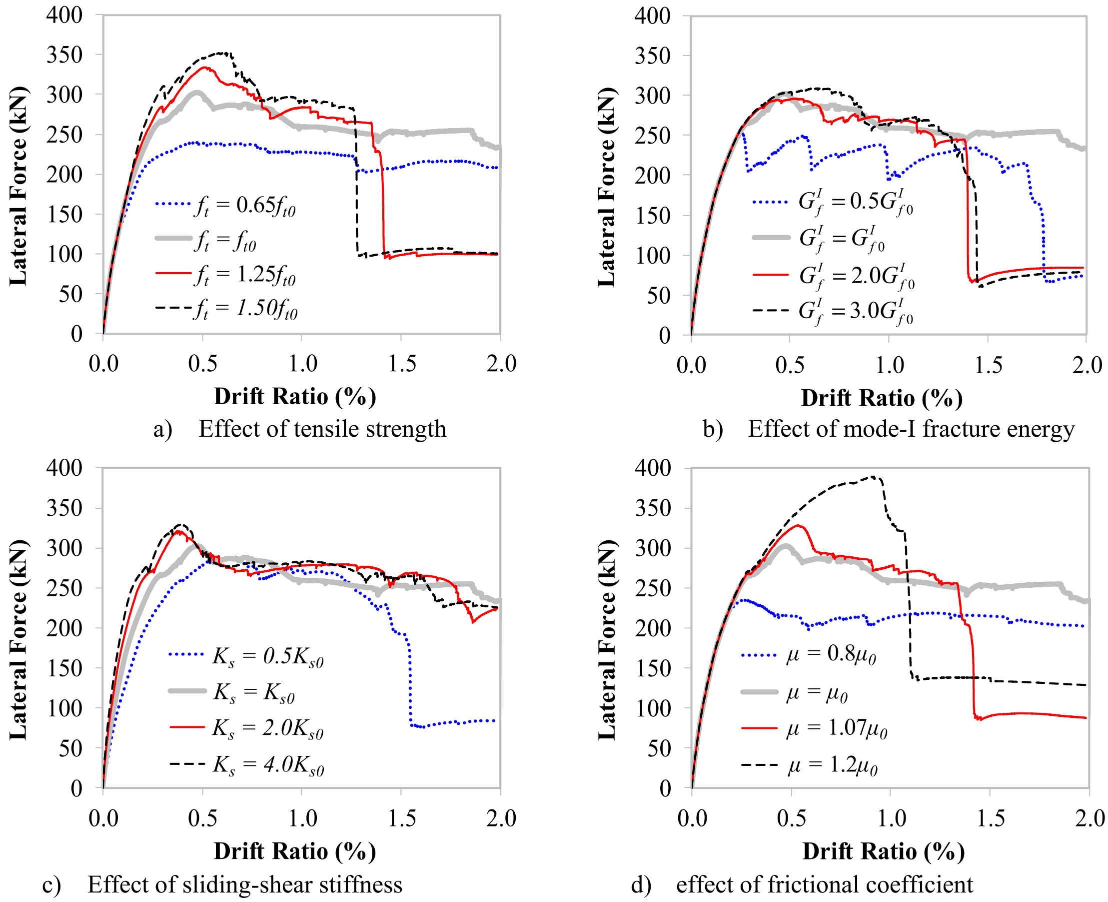

Fig. 20. Effect of material parameters of mortar interfaces on the obtained analysis results.

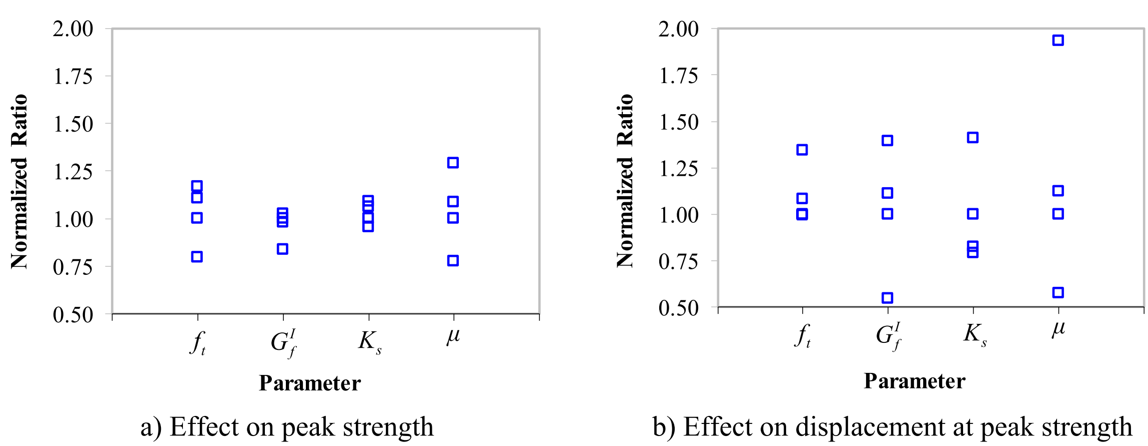

Fig. 21. Effect of parameters of zero-length macroelements on analytical results.

parameters, f_t and μ, of the interface obviously allow the infill frame to reach higher values of peak resistance; for a given value of stiffness, an increased peak resistance corresponds to an increased deformation at the peak. An increase in the fracture energy G_f^I leads to a strength increase or to a more ductile response. Consequently, an increased fracture energy leads to increased drift at peak. Finally, a reduction in the stiffness parameter K_s leads to a more flexible response, thus leading to an increased drift value at the peak resistance. Figure 22 indicates that the obtained inelastic deformability has a dependence on the material parameters. An increase in f_t or μ leads to a more brittle behavior, and this entails a lower deformability. The fracture energy G_f^I also affects the deformability, although its effect is less pronounced than that of other parameters. The stiffness parameter K_s also has an effect, because an increase in this parameter reduces the pre-peak flexibility of the model. Thus, strength degradation initiates at lower drift values for increased values of K_s.

4. Discussion

The proposed modeling approach has been shown to be capable of capturing the lateral load–displacement response and the damage pattern of infilled frames subjected to monotonic lateral loads. The modeling scheme is characterized by conceptual simplicity compared to

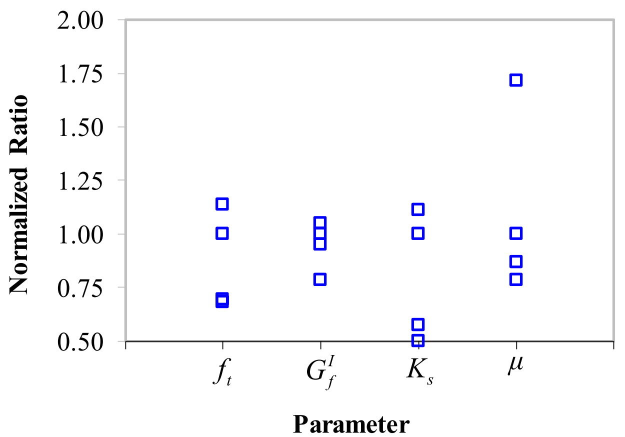

Fig. 22. Effect of parameters of zero-length macroelements on analytically obtained inelastic deformability.

refined finite element models, since it essentially relies on uniaxial constitutive laws for the concrete, reinforcing steel, masonry material and mortar joint interfaces. Despite this conceptual simplicity, the accuracy of the obtained analytical results is comparable to that obtained by Stavridis and Shing [50] with much more refined and computationally demanding finite element models. The analyses pursued herein use constitutive laws and element formulations which are readily available in *OpenSees*. This ensures that engineers and researchers will be able to use the proposed methodology, without a need to resort to commercial software or to implement user-defined capabilities in open-source software. The proposed analysis method constitutes an intermediate solution, between overly simplified, strut-based models, and overly complicated, nonlinear finite element models.

The adoption of the method in engineering practice entails two potential challenges. The first challenge involves the need to calibrate the constitutive laws for the truss elements representing the concrete members, masonry units and reinforcing bars, and for the spring elements representing the mortar interfaces. This difficulty can be addressed, as most of the material parameters pertain to uniaxial strength values; these can be determined through material testing or estimated (based on, e.g., nominal material properties), in accordance with the descriptions provided in evaluation documents such as the ASCE 41–17 [3]. In the absence of material test data for the strength of the mortar joint interfaces, the values used in this paper can be adopted; ideally, the adoption of these values must be supported by validation analyses using specimens which are not considered in the present study. The second potential challenge is related to the need to establish the truss-and-spring element assemblage of an infilled frame; this task may become overly cumbersome for analysis of multi-story, multi-bay frames. This issue can be easily resolved through implementation of user-friendly tools which can automatically generate the element assemblage for a given infilled frame. In fact, such an implementation has already been conducted for the truss modeling of RC members, as described in detail in Deng et al. [13]. In the specific approach, schematically summarized in Fig. 23a, each truss cell, consisting of two horizontal, two vertical and two inclined truss elements, is represented as a rectangular shell macroelement, substantially simplifying the pre-processing and post-processing of a truss model. The specific user-friendly implementation has enabled the efficient fully nonlinear analysis of three-dimensional building systems, as presented in Mavros et al. [32] and illustrated in Fig. 23b. A similar user-friendly formulation is feasible for the element assemblages of the infill walls, and it will enable the widespread adoption of the proposed analysis method by professional practice.

The element formulations and truss geometry used in the present study can also be employed for the analysis of infilled RC frames under cyclic lateral loading. Several enhancements to the constitutive laws may be deemed necessary for cyclic loading. The most important enhancement that is deemed necessary is the coupling of the normal and shear cohesive strengths, by means of a failure surface accounting for mixed-mode fracture. Other aspects of interface behavior that cannot be captured by the proposed macroelement-based approach are the irreversible normal compaction due to smoothening of the asperities in the mortar interfaces, and the reversible geometric dilatation effect [23].

5. Conclusions

A new method, based on the nonlinear truss analogy, has been presented for the analysis of masonry-infilled reinforced concrete (RC) frames. The RC members and the masonry units are represented through assemblages of horizontal, vertical and inclined truss elements. The truss representation of the frame members is based on a previously proposed method, which has been shown to be capable of capturing the inelastic response and the shear failure of RC columns. A procedure to define the truss geometry for the brick units has been established. The mortar joints and infill-to-frame interfaces are explicitly modeled by means of zero-length macroelements, that can account for mode-I and mode-II fracture and for frictional (Coulomb) shear sliding along mortar interfaces. The method has been validated with the results of monotonic tests on infilled frame specimens. The capability of the method to provide satisfactory estimates of the load–displacement response and of the damage patterns has been demonstrated. The validation analyses have been accompanied by a sensitivity study to determine the impact of several parameters of the zero-length macroelements on the analytical results. Overall, the friction coefficient and the tensile resistance of the

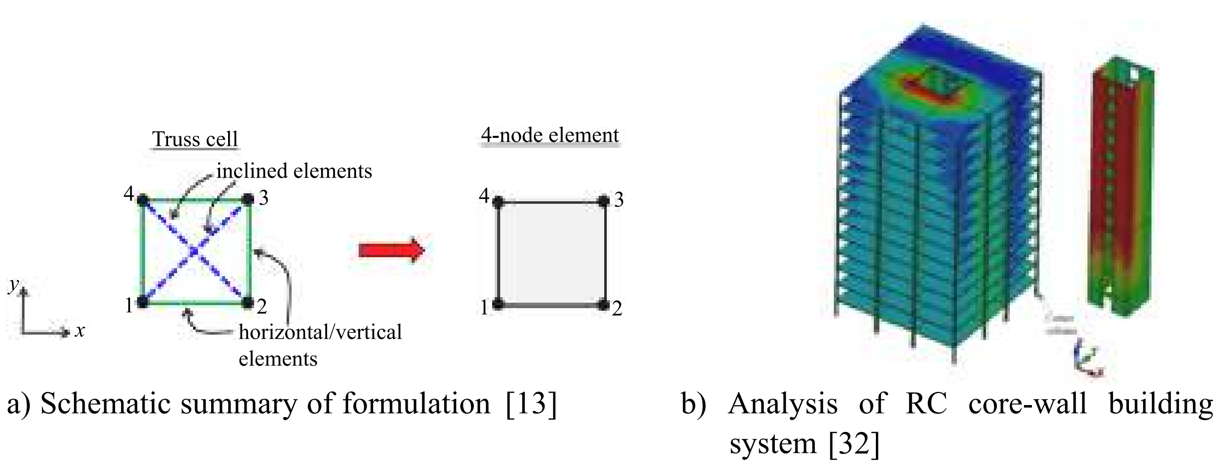

Fig. 23. Implementation of truss model as a shell macro-element.

mortar interfaces have been found to have the greatest influence on the peak lateral strength. The impact of model parameters on deformation quantities, such as the drift at peak lateral force, is greater than that on the peak strength. The proposed method constitutes an intermediate solution between overly simplified, strut-based models and overly complicated, nonlinear finite element models.

CRediT authorship contribution statement

Daniel Salinas: Methodology, Visualization, Writing – review & editing. **Ioannis Koutromanos:** Methodology, Visualization, Supervision, Writing – review & editing. **Roberto Leon:** Funding acquisition, Methodology, Supervision.

Declaration of Competing Interest

The authors declare that they have no known competing financial interests or personal relationships that could have appeared to influence the work reported in this paper.

Acknowledgements

The authors would like to thank TNO Diana for providing a one-year license agreement to perform finite element simulations and Dr. Mohammadreza Moharrami for providing post-processing tools for *OpenSees*, which enabled the graphical presentation of the evolution of the analytically obtained damage patterns. The first author's doctoral studies were partially funded by the Colombian government and private entities through grants COLFUTURO (PCB 2011-2 - 2012-2) and COLCIENCIAS (568: 2013-1 - 2016-1).

References

[1] Al-Chaar G. 2002. "Evaluating Strength and Stiffness of Unreinforced Masonry Infill Structures," *Research Report, US Army Corps of Engineering.*
[2] Al-Chaar G, Mehrabi AB, Manzouri T. Finite Element Interface Modeling and Experimental Verification of Masonry-Infilled R/C Frames. Masonry Society Journal 2008;26:47–66.
[3] ASCE 2017. "Seismic Evaluation and Retrofit of Existing Buildings – ASCE 41-17," *American Society of Civil Engineers.* ASCE, Reston, VA.
[4] Asteris PG, Antoniou ST, Sophianopoulos DS, Chrysostomou CZ. Mathematical Macromodeling of Infilled Frames: State of the Art. Journal of Structural Engineering ASCE 2011;137:1508–17.
[5] Bazant ZP, Planas J. Fracture and Size Effect in Concrete and other Quasibrittle Materials. Boca Raton, FL: CRC Press; 1998.
[7] Bose S, Martin J, Stavridis A. Framework for the nonlinear dynamic simulation of the seismic response of infilled RC frames. Los Angeles, California: on Earthquake Engineering; 2018.
[8] Breveglieri M, Camata G, Spacone E. Strengthened infilled RC frames: Continuum and macro modeling in nonlinear finite element analysis. Compos B Eng 2018;151: 78–91. https://doi.org/10.1016/j.compositesb.2018.05.042.
[9] Brodsky A, Huang Xu. Multi-platform modelling of masonry infilled frames. Journal of Building Engineering 2021;43:102561. https://doi.org/10.1016/j.jobe.2021.102561.
[10] Burton H, Deierlein G. Simulation of Seismic Collapse in Nonductile Reinforced Concrete Frame Buildings with Masonry Infills. ASCE Journal of Structural Engineering 2014;140(8):A4014016.
[11] Coleman J, Spacone E. Localization Issues in Force-Based Frame Elements. ASCE *Journal of Structural Engineering* 2001;10(1061):1422–5.
[12] Crisafulli FJ, Carr AJ. Proposed Macro-Model For The Analysis of Infilled Frame Structures. Bulletin of the New Zealand Society for Earthquake Engineering 2007; 40(2):69–77.
[13] Deng X, Koutromanos I, Murcia-Delso J, Panagiotou M. Nonlinear truss models for strain-based seismic evaluation of planar RC walls. Earthquake Eng Struct Dyn 2021;50(11):2939–60. https://doi.org/10.1002/eqe.3480.
[14] Di Trapani F, Shing PB, Cavaleri L. Macroelement model for in-plane and out-of-plane responses of masonry infills in frame structures. J Struct Eng 2018;144(2): 04017198. https://doi.org/10.1061/(ASCE)ST.1943-541X.0001926.
[15] Di Trapani F, Malavisi M. Seismic fragility assessment of infilled frames subject to mainshock/aftershock sequences using a double incremental dynamic analysis approach. Bull Earthq Eng 2019;17(1):211–35. https://doi.org/10.1007/s10518-018-0445-2.
[16] Filippou F, Popov E. & Bertero V. 1983. "Effects of Bond Deterioration on Hysteretic Behavior of Reinforced Concrete Joints," *Rep. EERC 83-19, Earthquake Engineering Research Center, Univ. of California, Berkeley.*
[17] Fiorato A. An Investigation of the Interaction of Reinforced Concrete Frames With Masonry Filler Walls. Department of Civil Engineering. University of Illinois at Urbana-Champaign; 1971.
[18] Hak S, Morandi P, Magenes G. Prediction of inter-storey drifts for regular RC structures with masonry infills based on bare frame modelling. Bull Earthq Eng 2018;16(1):397–425. https://doi.org/10.1007/s10518-017-0210-y.
[19] Huang H, Burton HB, Sattar S. Development and Utilization of a Database of Infilled Frame Experiments for Numerical Modeling. ASCE Journal of Structural Engineering 2020;146(6):04020079. https://doi.org/10.1061/(ASCE)ST.1943-541X.0002608.
[20] Hashemi A, Mosalam KM. Shake-table experiment on reinforced concrete structure containing masonry infill wall. Earthquake Eng Struct Dyn 2006;35(14):1827–52.
[21] Holmes M. Steel Frames with Brickwork and Concrete Infilling. ICE Proceedings 1961;19:473–8.
[22] Klingner RE, Bertero VV. Earthquake Resistance of Infilled Frames. Journal of the Structural Division 1978;104:973–89.
[23] Koutromanos I, Shing PB. Cohesive Crack Model to Simulate Cyclic Response of Concrete and Masonry Structures. ACI Struct J 2012;109:349–58.
[24] Koutromanos I, Shing PB. Numerical Modeling of Masonry-Infilled RC Frame Buildings. Berlin Heidelberg: Springer-Verlag; 2013. p. 123.
[25] Koutromanos I, Shing PB. Numerical Study of Masonry-Infilled RC Frames Retrofitted with ECC Overlays. J Struct Eng 2014;140(7):04014045. https://doi.org/10.1061/(ASCE)ST.1943-541X.0000934.
[26] Koutromanos I, Stavridis A, Shing PB, Willam K. Numerical Modeling of Masonry-Infilled RC Frames Subjected to Seismic Loads. Comput Struct 2011;89(11-12): 1026–37.
[27] Koutromanos I, Kyriakides M, Stavridis A, Billington S, Shing PB. Shake-Table Tests of A Three-Story Masonry-Infilled RC Frame Retrofitted with Composite Materials. ASCE Journal of Structural Engineering 2013;139(8):1340–51.
[28] Liberatore L, Noto F, Mollaioli F, Franchin P. In-plane response of masonry infill walls: Comprehensive experimentally-based equivalent strut model for deterministic and probabilistic analysis. Eng Struct 2018;167:533–48. https://doi.org/10.1016/j.engstruct.2018.04.057.
[29] Lourenço PB, Rots JG. Multisurface Interface Model for Analysis of Masonry Structures. ASCE Journal of Engineering Mechanics 1997;123(7):660–8.
[30] Lu Y, Panagiotou M. Three-Dimensional Cyclic Beam-Truss Model for Nonplanar Reinforced Concrete Walls. J Struct Eng 2014;140(3):04013071. https://doi.org/10.1061/(ASCE)ST.1943-541X.0000852.
[31] Mainstone RJ. On the Stiffness and Strengths of Infill Frames. Proceedings, The Institution of Civil Engineers 1971;49.
[32] Mavros M, Panagiotou M, Koutromanos I, Alvarez R, and Restrepo JI. 2022. "Seismic Analysis Of A Modern 14-Story RC Core Wall Building System Using The BTM-Shell Methodology," *Earthquake Engineering and Structural Dynamics*. https://onlinelibrary.wiley.com/doi/epdf/10.1002/eqe.3627.
[34] McKenna F, Fenves G, Scott M, Jeremic B. 2000. Open System for Earthquake Engineering Simulation, http:\\opensees.berkeley.edu.
[35] Mehrabi AB, Shing PB, Schuller M, Noland J. "Performance of masonry-infilled RC frames under in-plane lateral loads". *Report CUlSR-94-6*. Department of Civil, Environmental, and Architectura; Engineering. Boulder CO: University of Colorado; 1994.
[36] Mehrabi AB, Benson Shing P, Schuller MP, Noland JL. Experimental Evaluation of Masonry-infilled RC Frames. ASCE Journal of Structural Engineering 1996;122(3): 228–37.
[37] Mehrabi AB, Shing PB. Finite Element Modeling of Masonry-Infilled RC Frames. J Struct Eng 1997;123(5):604–13.
[38] Moharrami M, Koutromanos I, Panagiotou M, Girgin SC. Analysis of shear-dominated RC columns using the nonlinear truss analogy. Earthquake Eng Struct Dyn 2015;44(5):677–94.
[39] MSJC 2016. "Building Code Requirements and Specification for Masonry Structures," *MSJC (Masonry Standards Joint Committee)* (TMS 402/ACI 530/ASCE 5 and TMS 602/ACI 530.1/ASCE 6).
[40] Panagiotou M, Restrepo JI, Schoettler M, Kim G. Nonlinear Cyclic Truss Model for Reinforced Concrete Walls. ACI Struct J 2012;109:205–14.
[41] Papasotiriou A, Athanatopoulou A, Kostinakis K. Parametric study of the masonry infills' effect on the seismic performance of R/C frames based on the use of different damage measures. Eng Struct 2021;241:112326. https://doi.org/10.1016/j.engstruct.2021.112326.
[42] Pluijm RVD. "Material Properties of Masonry and Its Components Under Tension and Shear", *Proc.* In: Neis VV, editor. 6th Canadian Masonry Symposium. Saskatchewan. Canada: Saskatoon; 1992. p. 675–86.
[43] Polyakov SV. "On the Interaction Between Masonry Filler Walls and Enclosing Frame When Loaded in the Plane of the Wall", *Translations in Earthquake Engineering.* Earthquake Engineering Research Institute San Francisco 1960:36–42.
[44] Redmond L, Ezzatfar P, DesRoches R, Stavridis A, Ozcebe G, Kurc O. Finite Element Modeling of a Reinforced Concrete Frame with Masonry Infill and Mesh Reinforced Mortar Subjected to Earthquake Loading. Earthquake Spectra 2016;32(1):393–414.
[45] Sattar S. Influence of masonry infill walls and other building characteristics on seismic collapse of concrete frame buildings. Boulder: University of Colorado; 2013. Ph.D. Thesis.
[46] Sattar S, Liel AB. Seismic Performance of Nonductile Reinforced Concrete Frames with Masonry Infill Walls—II: Collapse Assessment. Earthquake Spectra 2016;32 (2):819–42.
[47] Schellenberg A. "Flat Slider Bearing Element", *opensees.berkeley.edu/wiki*. Berkeley: University of California; 2012.
[48] Stafford Smith B. Methods for Predicting the Lateral Stiffness and Strength of Multi-Storey Infilled Frames. Build Sci 1967;2(3):247–57.

[49] Stavridis A. Analytical and Experimental Study of Seismic Performance of Reinforced Concrete Frames Infilled with Masonry Walls. San Diego: Department of Structural Engineering, University of California; 2010. PhD thesis.
[50] Stavridis A, Shing PB. Finite-element modeling of nonlinear behavior of masonryinfilled RC frames. J Struct Eng 2010;136(3):285–96.
[51] Stavridis A, Koutromanos I, Shing PB. Shake-table tests of a three-story reinforced concrete frame with masonry infill walls. Earthquake Eng Struct Dyn 2012;41(6):1089–108.
[52] Stavridis A, Martin J. and Bose S. 2017. "Updating the ASCE 41 provisions for infilled RC frames," *Proceedings of the 2017 Structural Engineers Association of California (SEAOC) Convention*. Sacramento, CA.
[53] TNO (2014). "Building and Construction Research (TNO)," *DIANA, software, Delft, Netherlands,* available at http://tnodiana.com/content/DIANA.
[54] Vecchio FJ, Collins MP. The Modified Compression-Field Theory for Reinforced Concrete Elements Subjected to Shear. ACI 1986;83:219–31.
[55] Zarnic R, Gostic S. Non-linear Modelling of Masonry Infilled Frames. Proceedings 11th European Conference on Earthquake Engineering. 1998.

Further reading

[6] Bolis V, Stavridis A, Preti M. Numerical investigation of the in-plane performance of masonry-infilled RC frames with sliding subpanels. ASCE Journal of Structural Engineering 2017;143(2):04016168. https://doi.org/10.1061/(ASCE)ST.1943-541X.0001651.
[33] Milanesi RR, Morandi P, Magenes G. Local effects on RC frames induced by AAC masonry infills through FEM simulation of in-plane tests. Bull Earthq Eng 2018;16(9):4053–80. https://doi.org/10.1007/s10518-018-0353-5.